

# Finite Size Effects of the Surface States in a Lattice Model of Topological Insulator

Kazuto Ebihara, Keiji Yada, Ai Yamakage, and Yukio Tanaka

*Department of Applied Physics, Nagoya University, 464-8603, Japan*

---

## Abstract

Energy gap and wave function in thin films of topological insulator is studied, based on tight-binding model. It is revealed that thickness dependence of the magnitude of energy gap is composed of damping and oscillation. The damped behavior originates from the presence of gapless surface Dirac cone in the infinite thickness limit. On the other hand, the oscillatory behavior stems from electronic properties in the thin thickness limit.

*Keywords:*

Topological Insulator, Thin Film, Surface States,  $\text{Bi}_2\text{Se}_3$ , Finite-Size Effects

---

## 1. Introduction

Recently topological insulator has attracted much attention [1, 2, 3, 4, 5]. Topological insulator has been firstly predicted in a graphene with spin-orbit interaction [6], which consists of two copies of quantum Hall system, and shows a quantized spin Hall effect if  $z$ -component of spin of electrons is conserved. Generally speaking, the present non-trivial system is characterized by  $\mathbb{Z}_2$ -index introduced by Fu, Kane, and Mele [7, 8], and has a gapless helical edge mode where spin current protected by time-reversal symmetry flows spontaneously. However, quantum spin Hall (QSH) phase of graphene has not been observed experimentally since the spin-orbit interaction that is the driving force of topological insulator is much small. After that,  $\text{HgTe}/\text{HgCdTe}$  quantum well has been theoretically proposed as a candidate of two-dimensional topological insulator [9], and confirmed experimentally [10, 11, 12]. Topological insulators have been realized in three dimensional systems [13, 14, 15], *e.g.*,  $\text{Bi}_{1-x}\text{Sb}_x$  alloy [16], the binary compounds  $\text{Bi}_2\text{Se}_3$ ,  $\text{Bi}_2\text{Te}_3$  [17, 18, 19, 20], and TI-based ternary compound  $\text{TlBiSe}_3$  [21, 22, 23]. Furthermore, the quaternary compounds have also been theoretically predicted [24, 25]. All of these systems have a single helical Dirac cone on the surface.

Nowadays, many exotic quantum phenomena are expected originating from surface states of three-dimensional topological insulators [1, 2, 26, 27, 28, 29]. However, in the actual systems, sufficient amount of carriers remain in the bulk due to the difficulty of fabrication of samples [30]. Then the system becomes metallic and it is difficult to classify physical properties specific to surface Dirac cone [20, 31, 32]. To resolve this problem, several approaches, *e.g.*, chemical doping and surface adsorption [33] have been performed. The another new approach to control the carrier is to fabricate high quality thin films, where carrier control by gating is possible [34, 35]. But thin films may have the different electronic states from that of the bulk. Especially, the surface states have an energy gap due to the hybridization between the Dirac cones on top and bottom on the film induced by finite-size effect.

Based on above backgrounds, experimental studies of thin films of topological insulators have started [36, 37, 38]. Besides this, there have been many theoretical studies based on continuous models [39, 40, 41], first principle calculations [42, 43, 44, 45, 46], and tight-binding model calculation [42]. Although continuous model is simple, it is valid only for the long wavelength and low-energy limits. First principle calculation gives detailed electronic states of thin film. But it is difficult to analyze complicated phenomena, *e.g.*, transport properties, disorder effects, and quantum many-body problems. On the other hand, tight-binding approach is useful to calculate these interesting phenomena numerically, because many-body interaction and impurity effects are easily taken into account. However, electronic properties of thin film of topological insulator have not been fully studied based on tight-binding model.

In the present paper, we study electronic properties of thin film of  $\text{Bi}_2\text{Se}_3$  based on a tight-binding model focusing on the film-thickness dependencies of energy gap and surface states. It is revealed that the magnitude of energy gap is seriously influenced by material parameters. The paper is organized as follows. In section 2, we introduce a tight-binding model based on the Hamiltonian proposed by Refs. [17, 18]. In section 3, we calculate energy spectrum of thin film for various number of quintuple layers by changing material parameters. In section 4, we conclude our results.

## 2. Model

We use the effective model derived in Refs. [17, 18] as

$$H(\mathbf{k}) = \mathcal{E}(\mathbf{k}) + \begin{pmatrix} \mathcal{M}(\mathbf{k}) & 0 & B_0 k_z & A_0 k_- \\ 0 & \mathcal{M}(\mathbf{k}) & A_0 k_+ & -B_0 k_z \\ B_0 k_z & A_0 k_- & -\mathcal{M}(\mathbf{k}) & 0 \\ A_0 k_+ & -B_0 k_z & 0 & -\mathcal{M}(\mathbf{k}) \end{pmatrix}, \quad (1)$$

with

$$\mathcal{E}(\mathbf{k}) = C_0 + C_1 k_z^2 + C_2(k_x^2 + k_y^2), \quad (2)$$

$$\mathcal{M}(\mathbf{k}) = M_0 + M_1 k_z^2 + M_2(k_x^2 + k_y^2), \quad (3)$$

where  $k_{\pm} = k_x \pm i k_y$ , and the base is taken as  $(|+, \uparrow\rangle, |+, \downarrow\rangle, |-, \uparrow\rangle, |-, \downarrow\rangle)$ , in which  $\pm$  and  $\uparrow$  ( $\downarrow$ ) denote the parity eigenvalue and spin respectively. Let us introduce the lattice model only with nearest neighbor hoppings in a tetragonal lattice with substitution as

$$k_i a_i \rightarrow \sin k_i a_i, \quad (k_i a_i)^2 \rightarrow 2(1 - \cos k_i a_i). \quad (4)$$

As a result, the bulk Hamiltonian is derived as

$$H(\mathbf{k}) = \tilde{\mathcal{E}}(\mathbf{k}) + \begin{pmatrix} \tilde{\mathcal{M}}(\mathbf{k}) & 0 & B_0 \sin k_z c & \bar{A}_- \\ 0 & \tilde{\mathcal{M}}(\mathbf{k}) & \bar{A}_+ & -B_0 \sin k_z c \\ B_0 \sin k_z c & \bar{A}_- & -\tilde{\mathcal{M}}(\mathbf{k}) & 0 \\ \bar{A}_+ & -B_0 \sin k_z c & 0 & -\tilde{\mathcal{M}}(\mathbf{k}) \end{pmatrix}, \quad (5)$$

where

$$\tilde{\mathcal{E}}(k_x, k_y) = \bar{C}_0 + 2\bar{C}_1(1 - \cos k_z c) + 2\bar{C}_2(2 - \cos k_x a - \cos k_y a), \quad (6)$$

$$\tilde{\mathcal{M}}(\mathbf{k}) = \bar{M}_0 + 2\bar{M}_1(1 - \cos k_z c) + 2\bar{M}_2(2 - \cos k_x a - \cos k_y a), \quad (7)$$

$$\bar{A}_{\pm}(k_x, k_y) = \bar{A}_0(\sin k_x a \pm i \sin k_y a), \quad (8)$$

with  $a_i$  ( $a \equiv a_x = a_y$ ,  $c \equiv a_z$ ) being the lattice constant along  $i$  ( $= x, y, z$ )–direction. The relation between the original parameters and those in the present model is

$$\begin{aligned} \bar{M}_0 &= M_0, \bar{C}_0 = C_0, \bar{M}_1 = M_1/c^2, \bar{C}_1 = C_1/c^2, \\ \bar{M}_2 &= M_2/a^2, \bar{C}_2 = C_2/a^2, \bar{A}_0 = A_0/a, \bar{B}_0 = B_0/c. \end{aligned} \quad (9)$$

In the following, we express the present Hamiltonian in real space along  $z$ –direction perpendicular to the quintuple layers to focus on the surface states. Here, translational invariance is satisfied for the direction parallel to the quintuple layers i.e.,  $x$ – and  $y$ –directions. Then  $k_x$  and  $k_y$  are good quantum numbers. We apply open boundary condition only along  $z$ –direction, i.e., the system is regarded as a one–dimensional chain for fixed  $(k_x, k_y)$ . This condition corresponds to (111) cleavage surface of actual  $\text{Bi}_2\text{Se}_3$  which is easily cleaved. The corresponding Hamiltonian is given as follows,

$$\begin{aligned} H(k_x, k_y) &= \sum_{n=1}^{N_z} c_n^\dagger(k_x, k_y) H_0(k_x, k_y) c_n(k_x, k_y) \\ &\quad + \sum_{n=1}^{N_z-1} \left[ c_n^\dagger(k_x, k_y) H_1 c_{n+1}(k_x, k_y) + \text{h.c.} \right], \end{aligned} \quad (10)$$

where  $N_z$  denotes number of quintuple layers. It is noted that a lattice point  $n$  in the above Hamiltonian corresponds to position of a quintuple layer in the actual crystal structure. The on-site energy is given by

$$H_0(k_x, k_y) = \begin{pmatrix} \bar{M} + \bar{\mathcal{E}} & 0 & 0 & \bar{A}_- \\ 0 & \bar{M} + \bar{\mathcal{E}} & \bar{A}_+ & 0 \\ 0 & \bar{A}_- & -\bar{M} + \bar{\mathcal{E}} & 0 \\ \bar{A}_+ & 0 & 0 & -\bar{M} + \bar{\mathcal{E}} \end{pmatrix}, \quad (11)$$

with

$$\bar{\mathcal{E}}(k_x, k_y) = \bar{C}_0 + 2\bar{C}_1 + \bar{C}_2(2 - \cos k_x a - \cos k_y a), \quad (12)$$

$$\bar{M}(k_x, k_y) = \bar{M}_0 + 2\bar{M}_1 + \bar{M}_2(2 - \cos k_x a - \cos k_y a), \quad (13)$$

and the hopping between the nearest layers is as follows

$$H_1 = \begin{pmatrix} -\bar{M}_1 - \bar{C}_1 & 0 & i\bar{B}_0/2 & 0 \\ 0 & -\bar{M}_1 - \bar{C}_1 & 0 & -i\bar{B}_0/2 \\ i\bar{B}_0/2 & 0 & \bar{M}_1 - \bar{C}_1 & 0 \\ 0 & -i\bar{B}_0/2 & 0 & \bar{M}_1 - \bar{C}_1 \end{pmatrix}. \quad (14)$$

Since the Hamiltonian  $H(k_x, k_y)$  has an inversion symmetry, it follows that  $[H, P] = 0$ , or equivalently  $PH(k_x, k_y)P^{-1} = H(-k_x, -k_y)$ , where the parity operator  $P$  is defined by

$$P = \sum_{n=1}^{N_z} c_n^\dagger(k_x, k_y) \text{diag}[1, 1, -1, -1] c_{N_z+1-n}(k_x, k_y). \quad (15)$$

By using the parity operator  $P$ , we can derive the topological invariants  $\nu$ , which can be deduced from the parity of each pair of Kramers degenerate occupied energy band at the four time-reversal points at  $\Gamma_\alpha$  ( $\Gamma_1 = (0, 0)$ ,  $\Gamma_2 = (\pi, 0)$ ,  $\Gamma_3 = (0, \pi)$ ,  $\Gamma_4 = (\pi, \pi)$ ), in the Brillouin zone,

$$(-1)^\nu = \prod_{\alpha=1}^4 \prod_{m=1}^{N_z} \langle \phi_{2m}(\Gamma_\alpha) | P | \phi_{2m}(\Gamma_\alpha) \rangle, \quad (16)$$

where  $\phi_m(\Gamma_\alpha)$  is the eigenvector of the Hamiltonian  $H(\Gamma_\alpha)$ , and  $\langle \phi_m(\Gamma_\alpha) | P | \phi_m(\Gamma_\alpha) \rangle (= \pm 1)$  is the eigenvalue of parity operator  $P$ .

### 3. Results and discussions

We numerically obtain the eigenvalues and eigenvectors of bulk and surface states, diagonalizing the Hamiltonian given by eq. (10). The value of parameters  $\bar{M}_0, \bar{M}_2, \bar{A}_0, \bar{C}_0, \bar{C}_2$  are the same as in Ref. [18] with using  $a = 4.14\text{\AA}$ . The values of  $\bar{M}_1$  and  $\bar{C}_1$  are determined so that the eigen-energy at  $Z$ -point in Brillouin zone coincides with that of first principle calculation in Ref. [18]. The value of  $\bar{B}_0$  is chosen in order to fit the dispersion along  $\Gamma - Z$  line as well as possible. The indirect energy gap in the bulk Hamiltonian is located between  $-0.071\text{ eV}$  and  $|\bar{M}_0 + \bar{C}_0| = 0.29\text{ eV}$ , as derived from eq. (5).

Figure 1 shows the energy spectrum for a slab geometry in the cases of  $N_z = 3, 5, 9$ , and  $16$ . We can clearly see that eigenstates exist within the bulk energy gap. These states can be regarded as surface states, which we can directly confirm from its density distribution localized in the vicinity of surface, as shown in Figure 3. The surface states have a large magnitude of energy gap  $E_g \sim 0.033\text{ eV}$  for  $N_z = 3$  since the two wave functions localized at the top and bottom surfaces overlap significantly. (see (a) in Figure 1). The magnitude of the present energy gap becomes small with the increase of  $N_z$ . ((b) and (c) in Fig. 1.) For  $N_z = 16$ , the resulting  $E_g$  is significantly reduced to be  $0.15 \times 10^{-6}\text{ eV}$  ((d) in Figure 1). Moreover, it is noted that the shape of valence subband depends on  $N_z$ . For  $N_z = 3$  ((a) in Fig. 1), there are two valence subbands in  $-0.4\text{ eV} < E < 0\text{ eV}$ . The upper subband consists mainly of surface

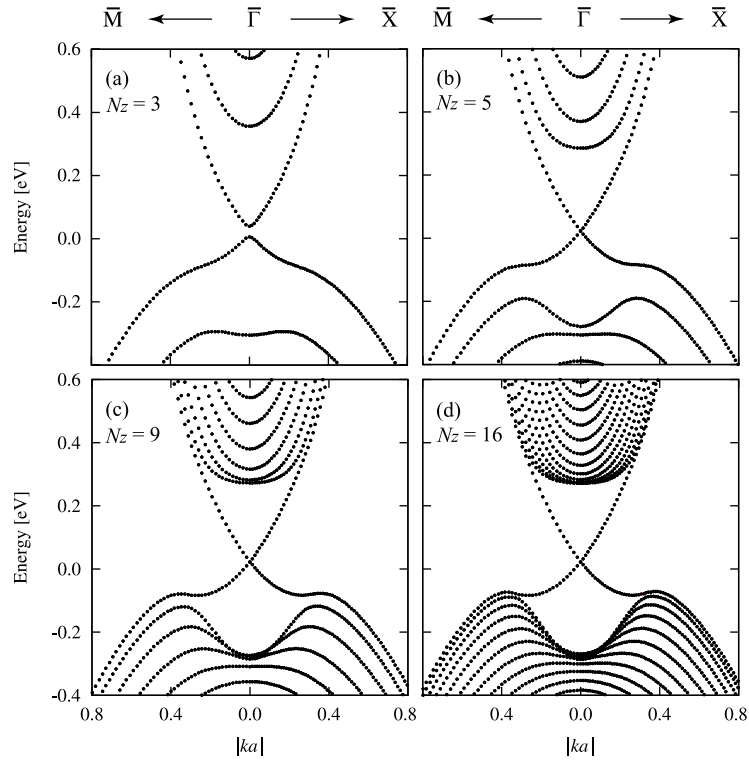


Figure 1: Energy spectra of the bulk and surface states near  $\bar{\Gamma}$ -point in the slab geometry for  $N_z = 3, 5, 9$ , and 16 quintuple layers. The material parameters are set as  $\bar{M}_0 = -0.28$  eV,  $\bar{M}_1 = 0.216$  eV,  $\bar{M}_2 = 2.60$  eV,  $\bar{A}_0 = 0.80$  eV,  $\bar{B}_0 = 0.32$  eV,  $\bar{C}_0 = -0.0083$  eV,  $\bar{C}_1 = 0.024$  eV,  $\bar{C}_2 = 1.77$  eV,  $a = 4.14$  Å, and  $c = 9.55$  Å.

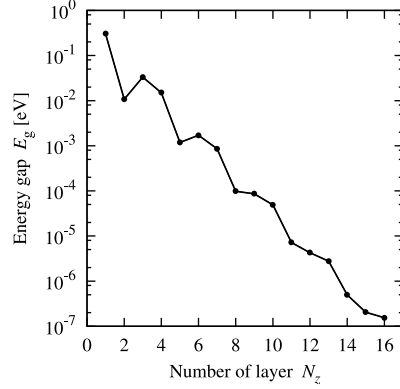


Figure 2: The magnitude of energy gap  $E_g$  of the surface state as a function of  $N_z$ . The material parameters are the same as in Figure 1.

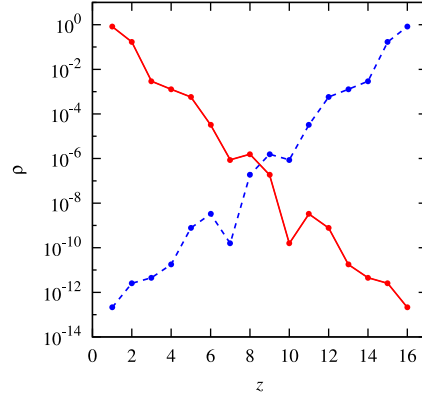


Figure 3: Density distribution  $\rho(z)$  of surface state at  $(k_x a, k_y a) = (\pi/32, \pi/32)$  for  $N_z = 16$ . There are two surface states located at the top and bottom in the system.  $z$  denotes the position of layer. The guided lines are drawn for view-ability. The material parameters are the same as in Figure 1.

states since it is located in the bulk energy gap. The lower one, that is bulk energy band, is located at  $\sim -0.3\text{eV}$ . The new subband appears between these two subbands at  $\sim -0.2\text{eV}$  for  $N_z = 5$  ((b) in Fig. 1). Simultaneously, valence subbands have a local minimum at  $k = 0$ , and an indirect energy gap is generated. For  $N_z = 9$  ((c) in Fig. 1) there are much more subbands. The energy bands for  $N_z = 16$  as shown in (d) in Fig. 1 is almost similar to that of bulk three-dimensional topological insulator with  $N_z \rightarrow \infty$ .

In Figure 2,  $N_z$  dependence of  $E_g$  is plotted. Hamiltonian of the monolayer system with  $N_z = 1$  is given by  $H_0(k_x, k_y)$  (see eq. (11)), which is equivalent to that of HgTe/HgCdTe quantum well [9], and  $E_g$  is given by  $2|\bar{M}_0 + 2\bar{M}_1| (= 0.30\text{eV})$ .  $E_g$  for  $N_z = 2$  is also derived analytically as  $|2\bar{M}_1 - [\bar{B}_0^2 + 4(\bar{M}_0 + 2\bar{M}_1)^2]^{1/2}| (= 0.0094\text{eV})$ . For  $N_z = 2, 3$ , and  $4$ ,  $E_g$  decreases roughly exponentially as a function of  $N_z$ , and becomes  $E_g \sim 10^{-1}\text{eV}$ .  $E_g$  becomes much smaller than room temperature for  $N_z \geq 5$ . It is also noted that  $E_g$  has an oscillatory behavior as a function  $N_z$  whose period is almost 3. The similar behavior has been obtained based on continuous models [39, 40, 41] and first principle calculations [42, 43, 44, 45, 46].

Next, we investigate the relation between the magnitude of energy gap and wave functions. Figure 3 shows the density distribution of surface states for  $N_z = 16$ , which is defined by

$$\rho(z) = \langle c_z^\dagger(k_x, k_y) c_z(k_x, k_y) \rangle, \quad z = 1, \dots, N_z, \quad (17)$$

where the expectation value is evaluated for the surface state with momentum  $(k_x a, k_y a) = (\pi/32, \pi/32)$ . The solid (dashed) line denotes the density distribution of surface state located on the top  $z = 1$  (bottom  $z = 16$ ). The density distribution decays exponentially with oscillation whose period is nearly 3 quintuple layers. This period is almost the

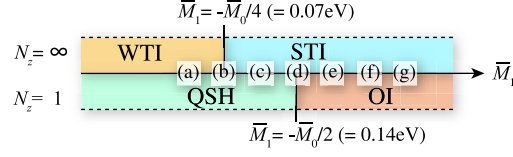


Figure 4: Phase diagrams of topological insulator for bulk limit  $N_z = \infty$  and for monolayer  $N_z = 1$ . STI (WTI) denotes strong (weak) topological insulator for  $N_z = \infty$ . QSH and OI denotes quantum spin Hall insulator where spin Hall conductance is quantized and ordinary insulator respectively for  $N_z = 1$ .  $\bar{M}_1 = 0.016, 0.070, 0.116, 0.140, 0.216, 0.316$ , and  $0.416\text{eV}$  for (a), (b), (c), (d), (e), (f), and (g), respectively. These values correspond to those used in Figure 5.

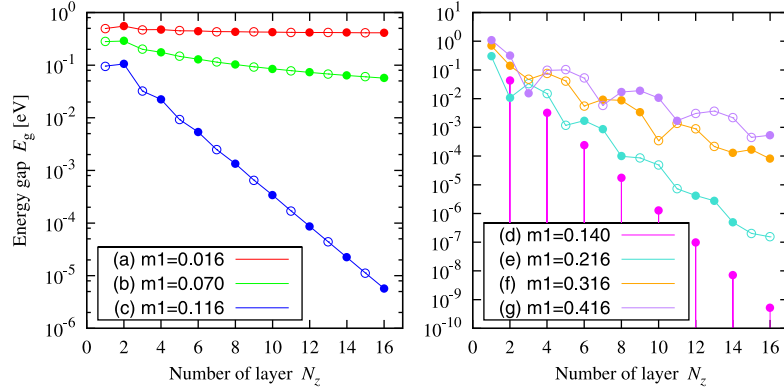


Figure 5: The magnitude of energy gap  $E_g$  as a function of  $N_z$  for different values of  $\bar{M}_1$ . The closed (open) circle describes a two-dimensional topological invariant  $\nu = 0 (\nu = 1)$ . At the case (d),  $E_g$  vanishes for odd numbers of layers:  $N_z = 1, 3, \dots, 15$ .

same as that of  $N_z$  dependence of  $E_g$ . Since the two wave functions located at the top and bottom surfaces oscillate spatially, the resulting  $E_g$  due to overlap between them also oscillates as a function of  $N_z$ .

In the following, we focus on the material parameters dependencies of  $E_g$ . For simplicity, we fix all parameters except for  $\bar{M}_1$ . Here, we choose seven cases of  $\bar{M}_1$  as shown in Figure 4. In order to understand electronic properties for the corresponding seven cases we have chosen, we show the phase diagram of the system for  $N_z = 1$  and  $N_z = \infty$  in Figure 4. In the limit for  $N_z = \infty$ , the system becomes weak topological insulator (WTI) for  $\bar{M}_1 < -\bar{M}_0/4 = 0.07\text{eV}$  while it becomes strong topological insulator (STI) for  $\bar{M}_1 > -\bar{M}_0/4 = 0.07\text{eV}$ . On the other hand, in the limit for  $N_z = 1$  the present system is QSH for  $\bar{M}_1 < -\bar{M}_0/2 = 0.14\text{eV}$ , while ordinary insulator (OI) for  $\bar{M}_1 > -\bar{M}_0/2 = 0.14\text{eV}$ .

Figure 5 shows  $E_g$  for various values of  $\bar{M}_1$ . The curve in Figure 1 coincides with the curve (e) obtained for  $\bar{M}_1 = 0.216\text{eV}$  in Figure 5, which is the same parameter as that of  $\text{Bi}_2\text{Se}_3$ . The curve (e) has a three-fold periodic damped oscillation. For  $\bar{M}_1 = 0.016\text{eV}$  (case (a) in Fig. 5), where the system is WTI (QSH) with  $N_z = \infty$  ( $N_z = 1$ ),  $E_g$  does not decay with the increase of  $N_z$  since there is no gapless surface Dirac cone at  $\bar{\Gamma}$ -point for  $N_z = \infty$ . For  $\bar{M}_1 = 0.070\text{eV}$  (case (b) in Fig. 5), which is the transition point between WTI and STI, where closing of the bulk energy gap occurs at  $\bar{\Gamma}$ -point,  $E_g$  decreases monotonically as a function of  $N_z$ . For  $\bar{M}_1 = 0.116\text{eV}$  (case (c) in Fig. 5),  $E_g$  decays exponentially except for  $N_z < 5$  as a function of  $N_z$ , since surface Dirac cone is generated with  $N_z = \infty$ .  $E_g$  has a strong oscillation for  $\bar{M}_1 = 0.140\text{eV}$  (case (d) in Fig. 5), where transition between OI and QSH occurs for  $N_z = 1$ .  $E_g$  becomes exactly zero for odd numbers of  $N_z$  (See Appendix). The damped oscillation with four-fold periodicity appears at  $\bar{M}_1 = 0.316\text{eV}$  (case (f) in Fig. 5) and at  $\bar{M}_1 = 0.416\text{eV}$  (case (g) in Fig. 5). When the system is QSH for  $N_z = 1$ ,  $E_g$  decreases monotonically in the wide parameter range of  $N_z$ . On the other hand,  $E_g$  shows a damped oscillation as a function of  $N_z$  for  $\bar{M}_1 > 0.140\text{eV}$ , *i.e.*, the system is OI in the thin thickness limit. As we have seen above, the period of oscillation depends on  $\bar{M}_1$ . It can be concluded that the  $N_z$  dependence of  $E_g$  is sensitive to the material parameter  $\bar{M}_1$ . We also show the topological invariant  $\nu$  in Fig. 5. The closed circle expresses non-topological phase with  $\nu = 0$ , while the open circle expresses topological phase with  $\nu = 1$ . For cases with (a), (b) and (c), non-topological phase emerges for even number of layers and topological phase emerges for odd number of

layers. Topological phase and non-topological phase appear oscillatory also for cases with (e), (f) and (g). However, the period of oscillation becomes three or four. These results are consistent with those by Liu *et al.* [42]. Since the magnitude of energy gap becomes zero at the boundary between topological and non-topological phases, the period of oscillation of topological number  $\nu$  coincides with that of the energy gap.

#### 4. Conclusion

We obtain the energy spectrum of surface states in a topological insulator based on tight-binding model. It is clarified that there are various types of thickness dependencies of  $E_g$ . The origin of the damped oscillatory behavior of  $E_g$  is partitioned into two parts. The damped behavior appears when the gapless surface Dirac cone is realized in the limit of  $N_z = \infty$ . The oscillatory behavior of  $E_g$  becomes prominent when the system approaches to OI regime for  $N_z = 1$ .

Based on these results, we would expect various types of thin films by controlling material parameters, which could be controlled by external pressure along z-direction (c-axis) for  $\text{Bi}_2\text{Se}_3$ . Tuning of material parameters may be much more easier for optical lattices made from cold atoms [47, 48, 49, 50, 51, 52]. If we can tune the corresponding material parameters with the case (d) in Fig.4, the strong even-odd effect is expected. In this case, various transport properties are sensitive to external fields. There are several future unresolved problems. The Anderson localizations of thin films have been recently studied [38, 53, 54] from various aspects. It is interesting to study this problem with various types of thin films with different electronic properties of topological insulator with different material parameters.

#### 5. Acknowledgments

This work was supported in part by a Grant-in-Aid for Scientific Research from MEXT of Japan, “Topological Quantum Phenomena” No. 22103005 and No. 22340096.

#### Appendix

As shown in Fig. 5, the energy gap is exactly zero for the odd number of layers, and non-zero for the even number of layers at the case (d) in Fig. 4. In the following, we derive this behavior of the energy gap. The Hamiltonian for  $N_z$  at  $\bar{\Gamma}$  point reads

$$H_{N_z}(0,0) = F_{N_z} + G_{N_z}, \quad (18)$$

with  $4N_z \times 4N_z$  matrices  $F_{N_z}$  and  $G_{N_z}$  being

$$F_{N_z} = \sum_{n=1}^{N_z} c_n^\dagger \text{diag}[(\bar{C}_0 + 2\bar{C}_1), \dots, (\bar{C}_0 + 2\bar{C}_1)] c_n \quad (19)$$

$$G_{N_z} = \sum_{n=1}^{N_z-1} [c_n^\dagger H_1 c_{n+1} + \text{h.c.}]. \quad (20)$$

where  $\bar{M}_0 + 2\bar{M}_1 = 0$  at the case (d). The eigenvalue of  $H_{N_z}(0,0)$  equals to  $\bar{C}_0 + 2\bar{C}_1 + E_n^G$  where  $E_n^G$  is the eigenvalue of  $G_{N_z}$ . If matrix  $G_{N_z}$  has zero eigenvalue, the energy gap closes because  $G_{N_z}$  has particle hole symmetry. We show  $|G_{N_z}| \equiv \det G_{N_z} = 0$  for odd number of  $N_z$  at  $\bar{\Gamma}$  point, as follows.

$$|G_{N_z}| = \begin{vmatrix} 0 & H_1 & 0 & & \\ H_1^\dagger & 0 & H_1 & & \\ 0 & H_1^\dagger & 0 & \ddots & \\ & & \ddots & \ddots & \ddots \\ & & & \ddots & 0 & H_1 \\ & & & & H_1^\dagger & 0 \end{vmatrix} = \begin{vmatrix} H_1 & 0 & 0 & & \\ 0 & H_1^\dagger & H_1 & & \\ H_1^\dagger & 0 & 0 & \ddots & \\ & & H_1^\dagger & \ddots & \ddots \\ & & & \ddots & 0 & H_1 \\ & & & & H_1^\dagger & 0 \end{vmatrix}$$

$$\begin{aligned}
&= |H_1| \begin{vmatrix} H_1^\dagger & H_1 & & \\ 0 & 0 & \ddots & \\ & H_1^\dagger & \ddots & \ddots \\ & & \ddots & 0 & H_1 \\ & & & H_1^\dagger & 0 \end{vmatrix} = |H_1|^2 \begin{vmatrix} 0 & H_1 & & \\ H_1^\dagger & \ddots & \ddots & \\ & \ddots & 0 & H_1 \\ & & H_1^\dagger & 0 \end{vmatrix} \\
&= |H_1|^2 |G_{N_z-2}|,
\end{aligned} \tag{21}$$

and we find

$$|G_{N_z=1}| = 0, \tag{22}$$

$$|G_{N_z=2}| = \begin{vmatrix} 0 & H_1 \\ H_1^\dagger & 0 \end{vmatrix} = |H_1|^2 \neq 0. \tag{23}$$

Thus the energy gap at the case (d) is exactly zero for the odd number of layers, and non-zero for the even number of layers, and oscillates strongly as a function of  $N_z$ .

## References

- [1] M. Z. Hasan, C. L. Kane, Rev. Mod. Phys. 82 (2010) 3045.
- [2] X.-L. Qi, S.-C. Zhang, Physics Today 63 (2010) 33.
- [3] X.-L. Qi, S.-C. Zhang, ArXiv:1008.2026 (2010).
- [4] J. Moore, Nature 464 (2010) 194.
- [5] M. Z. Hasan, D. Hsieh, Y. Xia, L. A. Wray, S.-Y. Xu, C. L. Kane, ArXiv:1105.0396 (2011).
- [6] C. L. Kane, E. J. Mele, Phys. Rev. Lett. 95 (2005) 226801.
- [7] C. L. Kane, E. J. Mele, Phys. Rev. Lett. 95 (2005) 146802.
- [8] L. Fu, C. L. Kane, Phys. Rev. B 74 (2006) 195312.
- [9] B. A. Bernevig, T. L. Hughes, S.-C. Zhang, Science 314 (2006) 1757.
- [10] M. König, S. Wiedmann, C. Brüne, A. Roth, H. Buhmann, L. W. Molenkamp, X.-L. Qi, S.-C. Zhang, Science 318 (2007) 766.
- [11] A. Roth, C. Brüne, H. Buhmann, L. W. Molenkamp, J. Maciejko, X.-L. Qi, S.-C. Zhang, Science 325 (2009) 294.
- [12] C. Brüne, A. Roth, H. Buhmann, E. M. Hankiewicz, L. W. Molenkamp, J. Maciejko, X.-L. Qi, S.-C. Zhang, ArXiv:1107.0585 (2011).
- [13] L. Fu, C. L. Kane, E. J. Mele, Phys. Rev. Lett. 98 (2007) 106803.
- [14] L. Fu, C. L. Kane, Phys. Rev. B 76 (2007) 045302.
- [15] J. E. Moore, L. Balents, Phys. Rev. B 75 (2007) 121306.
- [16] D. Hsieh, D. Qian, L. Wray, Y. Xia, Y. S. Hor, R. J. Cava, M. Z. Hasan, Nature 452 (2008) 970–974.
- [17] H. Zhang, C.-X. Liu, X.-L. Qi, X. Dai, Z. Fang, S.-C. Zhang, Nature Phys. 5 (2009) 438–442.
- [18] C.-X. Liu, X.-L. Qi, H. Zhang, X. Dai, Z. Fang, S.-C. Zhang, Phys. Rev. B 82 (2010) 045122.
- [19] Y. Xia, D. Qian, D. Hsieh, L. Wray, A. Pal, H. Lin, A. Bansil, D. Grauer, Y. S. Hor, R. J. Cava, M. Z. Hasan, Nature Phys. 5 (2009) 398–402.
- [20] Y. L. Chen, J. G. Analytis, J.-H. Chu, Z. K. Liu, S.-K. Mo, X.-L. Qi, H. J. Zhang, D. H. Lu, X. Dai, Z. Fang, S.-C. Zhang, I. R. Fisher, Z. Hussain, Z.-X. Shen, Science 325 (2009) 178.
- [21] B. Yan, C.-X. Liu, H.-J. Zhang, C.-Y. Yam, X.-L. Qi, T. Frauenheim, S.-C. Zhang, Europhys. Lett. 90 (2010) 37002.
- [22] H. Lin, R. S. Markiewicz, L. A. Wray, L. Fu, M. Z. Hasan, A. Bansil, Phys. Rev. Lett. 105 (2010) 036404.
- [23] T. Sato, K. Segawa, H. Guo, K. Sugawara, S. Souma, T. Takahashi, Y. Ando, Phys. Rev. Lett. 105 (2010) 136802.
- [24] S. Chen, X. G. Gong, C.-G. Duan, Z.-Q. Zhu, J.-H. Chu, A. Walsh, Y.-G. Yao, J. Ma, S.-H. Wei, Phys. Rev. B 83 (2011) 245202.
- [25] Y. J. Wang, H. Lin, T. Das, M. Z. Hasan, A. Bansil, ArXiv:1106.3316 (2011).
- [26] Y. Tanaka, T. Yokoyama, N. Nagaosa, Phys. Rev. Lett. 103 (2009) 107002.
- [27] J. Linder, Y. Tanaka, T. Yokoyama, A. Sudbo, N. Nagaosa, Phys. Rev. Lett. 104 (2010) 067001.
- [28] J. Linder, Y. Tanaka, T. Yokoyama, A. Sudbo, N. Nagaosa, Phys. Rev. B 81 (2010) 184525.
- [29] T. Yokoyama, Y. Tanaka, N. Nagaosa, Phys. Rev. B 81 (2010) 121401.
- [30] G. R. Hyde, H. A. Beale, I. L. Spain, J. A. Woollam, J. Phys. Chem. Solids 35 (1974) 1719–1728.
- [31] A. A. Taskin, Y. Ando, Phys. Rev. B 80 (2009) 085303.
- [32] J. G. Checkelsky, Y. S. Hor, M.-H. Liu, D.-X. Qu, R. J. Cava, N. P. Ong, Phys. Rev. Lett. 103 (2009) 246601.
- [33] D. Hsieh, Y. Xia, D. Qian, L. Wray, J. H. Dil, F. Meier, J. Osterwalder, L. Patthey, J. G. Checkelsky, N. P. Ong, A. V. Fedorov, H. Lin, A. Bansil, D. Grauer, Y. S. Hor, R. J. Cava, M. Z. Hasan, Nature 460 (2009) 1101–1105.
- [34] J. Chen, H. J. Qin, F. Yang, J. Liu, T. Guan, F. M. Qu, G. H. Zhang, J. R. Shi, X. C. Xie, C. L. Yang, K. H. Wu, Y. Q. Li, L. Lu, Phys. Rev. Lett. 105 (2010) 176602.
- [35] J. Chen, X. Y. He, K. H. Wu, Z. Q. Ji, L. Lu, J. R. Shi, J. H. Smet, Y. Q. Li, Phys. Rev. B 83 (2011) 241304.
- [36] Y. Zhang, K. He, C.-Z. Chang, C.-L. Song, L.-L. Wang, X. Chen, J.-F. Jia, Z. Fang, X. Dai, W.-Y. Shan, S.-Q. Shen, Q. Niu, X.-L. Qi, S.-C. Zhang, X.-C. Ma, Q.-K. Xue, Nature Phys. 6 (2010) 712.



- [37] Y. Sakamoto, T. Hirahara, H. Miyazaki, S.-i. Kimura, S. Hasegawa, Phys. Rev. B 81 (2010) 165432.
- [38] T. Hirahara, Y. Sakamoto, Y. Takeichi, H. Miyazaki, S.-i. Kimura, I. Matsuda, A. Kakizaki, S. Hasegawa, Phys. Rev. B 82 (2010) 155309.
- [39] J. Linder, T. Yokoyama, A. Sudbø, Phys. Rev. B 80 (2009) 205401.
- [40] H.-Z. Lu, W.-Y. Shan, W. Yao, Q. Niu, S.-Q. Shen, Phys. Rev. B 81 (2010) 115407.
- [41] W.-Y. Shan, H.-Z. Lu, S.-Q. Shen, New J. Phys. 12 (2010) 043048.
- [42] C.-X. Liu, H. Zhang, B. Yan, X.-L. Qi, T. Frauenheim, X. Dai, Z. Fang, S.-C. Zhang, Phys. Rev. B 81 (2010) 041307.
- [43] K. Park, J. J. Heremans, V. W. Scarola, D. Minic, Phys. Rev. Lett. 105 (2010) 186801.
- [44] O. V. Yazyev, J. E. Moore, S. G. Louie, Phys. Rev. Lett. 105 (2010) 266806.
- [45] H. Jin, J.-H. Song, A. J. Freeman, Phys. Rev. B 83 (2011) 125319.
- [46] J. Chang, L. F. Register, S. K. Banerjee, B. Sahu, Phys. Rev. B 83 (2011) 235108.
- [47] N. Goldman, I. Satija, P. Nikolic, A. Bermudez, M. A. Martin-Delgado, M. Lewenstein, I. B. Spielman, Phys. Rev. Lett. 105 (2010) 255302.
- [48] A. Bermudez, M. A. Martin-Delgado, D. Porras, New Journal of Physics 12 (2010) 123016.
- [49] A. Bermudez, D. Patanè, L. Amico, M. A. Martin-Delgado, Physical Review Letters 102 (2009) 135702.
- [50] A. Bermudez, L. Amico, M. A. Martin-Delgado, New Journal of Physics 12 (2010) 055014.
- [51] N. Goldman, A. Kubasiak, A. Bermudez, P. Gaspard, M. Lewenstein, M. A. Martin-Delgado, Phys. Rev. Lett. 103 (2009) 035301.
- [52] A. Bermudez, N. Goldman, A. Kubasiak, M. Lewenstein, M. A. Martin-Delgado, New Journal of Physics 12 (2010) 033041.
- [53] M. Liu, C.-Z. Chang, Z. Zhang, Y. Zhang, W. Ruan, K. He, L.-l. Wang, X. Chen, J.-F. Jia, S.-C. Zhang, Q.-K. Xue, X. Ma, Y. Wang, Phys. Rev. B 83 (2011) 165440.
- [54] J. Wang, A. M. DaSilva, C.-Z. Chang, K. He, J. K. Jain, N. Samarth, X.-C. Ma, Q.-K. Xue, M. H. W. Chan, Phys. Rev. B 83 (2011) 245438.